The Stannide $LiRh_3Sn_5$ – Synthesis, Structure, and Chemical Bonding

Puravankara Sreeraj[a], Dirk Johrendt[b], Helen Müller[b], Rolf-Dieter Hoffmann[a], Zhiyun Wu[a], and Rainer Pöttgen[a]

[a] Institut für Anorganische und Analytische Chemie, Sonderforschungsbereich 458 and NRW Graduate School of Chemistry, Westfälische Wilhelms-Universität Münster, Corrensstraße 36, D-48149 Münster (Germany)
[b] Department Chemie und Biochemie, Ludwig-Maximilians-Universität München, Butenandtstraße 5 – 13 (Haus D), D-81377 München, Germany

Reprint requests to R. Pöttgen. E-mail: pottgen@uni-muenster.de

Z. Naturforsch. **60b,** 933 – 939 (2005); received July 4, 2005

The lithium rhodium stannide $LiRh_3Sn_5$ was synthesized from the elements in a sealed tantalum tube and investigated *via* X-ray powder and single crystal diffraction: *Pbcm*, $a = 538.9(1)$, $b = 976.6(3)$, $c = 1278.5(3)$ pm, $wR2 = 0.0383$, 1454 F^2 values, and 44 variables. Refinement of the occupancy parameters revealed a lithium content of 92(6)%. $LiRh_3Sn_5$ crystallizes with a new structure type. The structure is built up from a complex three-dimensional $[Rh_3Sn_5]$ network, in which the lithium atoms fill channels in the *b* direction. The $[Rh_3Sn_5]$ network is governed by Rh–Rh (274 – 295 pm), Rh–Sn (262 – 287 pm), and Sn–Sn (289 – 376 pm) interactions. The lithium atoms have CN 13 (4 Rh + 9 Sn). Electronic band structure calculations and the COHP bond analysis reveal strong Rh−Sn bonds and also significant Rh−Rh bonding within the Rh_3Sn_5 network, which is additionally stabilized by weak but frequent Sn−Sn interactions.

Key words: Lithium Stannide, Crystal Chemistry, Chemical Bonding

Introduction

The binary lithium stannides have intensively been investigated with respect to their use as electrode materials in lithium-based batteries, since such intermetallic compounds significantly reduce the problem of whisker growth. An overview on these investigations is given in a review article [1] and some recent work [2 – 7]. Although a variety of ternary lithium transition metal stannides have been synthesized and structurally characterized [8 – 16], these materials have not yet been investigated with respect to potential lithium mobility. Recent examples for such investigations on ternary stannides are $LiTSn_4$ (T = Ru, Rh, Ir) [17 – 19], $LiAg_2Sn$ [20], $Li_{17}Ag_3Sn_6$ [16], Li_2AuSn_2 [21], LiAuSn [22, 23], and $LiAu_3Sn_4$ [23], the series $Li_{1+x}Pd_2Sn_{6-x}$ [24], $LiCoSn_6$ [25], and the solid solution $Li_{3-x}Pt_2Sn_{3+x}$ [26]. Especially for $LiAg_2Sn$ [20] and Li_2AuSn_2 [21], temperature dependent ^{7}Li solid state NMR investigations revealed low activation energies for lithium motion of 33 and 27 kJ/mol, respectively.

In continuation of our systematic investigations on the structures and properties of lithium transition metal stannides we obtained the new stannide $LiRh_3Sn_5$ with a complex three-dimensional $[Rh_3Sn_5]$ network. The structure determination and a detailed analysis of chemical bonding of this stannide are reported herein.

Experimental Section

Synthesis

Starting materials for the synthesis of $LiRh_3Sn_5$ were lithium rods (Merck, > 99.5%), rhodium powder (Degussa-Hüls, *ca.* 200 mesh, > 99.9%), and tin granules (Heraeus, > 99.9%). The lithium rods were cut into smaller pieces under dried (over lithium) paraffin oil. The lithium pieces were washed with *n*-hexane (dried over sodium wire) and the clean pieces were kept in Schlenk tubes under dry argon until use. The commercial argon (Westfalengas, 4.8) was purified over titanium sponge (970 K), silica gel, and molecular sieves.

Lithium pieces, rhodium powder, and tin granules were then weighed in the ideal 1:3:5 atomic ratio and arc-welded in a small tantalum tube (*ca.* 1 cm^3) under an argon pressure of *ca.* 800 mbar. Details on the arc-melting equipment are given elsewhere [27]. The tantalum tube was subsequently sealed in a quartz tube for oxidation protection and first heated at 970 K for two hours. After rapid cooling to 670 K, the sample was kept at that temperature for another two weeks and finally quenched by radiative heat loss outside the furnace. The product could easily be separated from the tan-

Table 1. Crystal data and structure refinement for $LiRh_3Sn_5$.

Empirical formula	$LiRh_3Sn_5$
Formula weight	909.12 g/mol
Unit cell dimensions	$a = 538.9(1)$ pm
	$b = 976.6(3)$ pm
	$c = 1278.5(3)$ pm
	$V = 0.6729$ nm^3
Pearson symbol	oP36
Structure type	$LiRh_3Sn_5$
Space group	*Pbcm*
Formula units per cell	$Z = 4$
Calculated density	8.97 g/cm^3
Crystal size	$40 \times 40 \times 130$ μm^3
Transmission ratio (max/min)	0.447 : 0.150
Absorption coefficient	25.3 mm^{-1}
F(000)	1552
Detector distance	60 mm
Exposure time	12 min
ω Range; increment	$0-180^\circ$, 1.0°
Integration parameters A, B, EMS	14.5, 4.5, 0.020
θ Range for data collection	3° to 35°
Range in *hkl*	± 8, ± 15, ± 20
Total no. of reflections	9359
Independent reflections	1454 ($R_{int} = 0.0323$)
Reflections with $I > 2\sigma(I)$	1389 ($R_\sigma = 0.0172$)
Data / parameters	1454 / 44
Goodness-of-fit on F^2	1.383
Final R indices $[I > 2\sigma(I)]$	$R1 = 0.0220$; $wR2 = 0.0378$
R Indices (all data)	$R1 = 0.0247$; $wR2 = 0.0383$
Extinction coefficient	0.0162(3)
Largest diff. peak and hole	1.36 and -1.93 e/Å^3

talum tube by mechanical fragmentation. No reaction with the crucible material could be observed. $LiRh_3Sn_5$ is stable in air over weeks. Polycrystalline pieces are light grey with metallic lustre.

X-ray film data and structure refinements

The samples have been analyzed through Guinier powder patterns using Cu-$K_{\alpha 1}$, radiation and α-quartz ($a = 491.30$; $c = 540.46$ pm) as an internal standard. The Guinier camera was equipped with an image plate system (Fujifilm, BAS-1800). The orthorhombic lattice parameters (Table 1) were refined from the Guinier data. The correct indexing of the pattern was facilitated through an intensity calculation [28], taking the atomic positions obtained from the structure refinement. The lattice parameters determined for the powder and the different single crystals agreed well.

Small, irregularly-shaped single crystals were selected from the crushed samples and mounted on small glass fibres using bees wax. They were first examined on a Buerger camera (equipped with the same image plate system) *via* Laue photographs in order to check the crystal quality for intensity data collection.

Intensity data were collected at room temperature on a Stoe IPDS-II diffractometer in oscillation mode using graphite monochromatized Mo-K_α radiation. A numerical absorption correction was applied to the data. All relevant crystallographic data and details for the intensity data collection are listed in Table 1. Careful analysis of the image plate data set revealed a primitive orthorhombic unit cell, and the systematic extinctions were compatible with space group *Pbcm*. The positions of the rhodium and tin atoms were deduced from an automatic interpretation of direct methods using SHELXS-97 [29]. The lithium site was obtained from a subsequent difference Fourier synthesis. The rhodium and tin sites were refined with anisotropic atomic displacement parameters, while the lithium site was refined isotropically. The refinement was performed with SHELXL-97 (full-matrix least-squares on F^2) [30]. Since rhodium and tin differ only by five electrons, the occupancy parameters of these five sites were refined in a separate series of least-squares cycles in order to check for the correct site assignments. These sites were fully occupied within two standard uncertainties, and in the subsequent cycles, the ideal occupancies were assumed again. There was no hint for Rh/Sn mixing. The quality of the data set allowed also a refinement of the lithium occupancy parameter. The refined value of 92(6)% lithium indicates only small defects. Since this site also is fully occupied within two standard uncertainties, the ideal $LiRh_3Sn_5$ composition was assumed for the final cycles. The refinement went smoothly to the residuals listed in Table 1. A final difference Fourier synthesis (Table 1) was flat. The refined atomic coordinates and interatomic distances are listed in Tables 2 and 3. Further details on the structure refinement can

Table 2. Atomic coordinates and anisotropic displacement parameters (pm^2) for $LiRh_3Sn_5$. U_{eq} is defined as one third of the trace of the orthogonalized U_{ij} tensor. The anisotropic displacement factor exponent takes the form: $-2\pi^2[(ha^*)^2U_{11} + \ldots + 2hka^*b^*U_{12}]$.

Atom	Wyckoff position	x	y	z	U_{11}	U_{22}	U_{33}	U_{23}	U_{13}	U_{12}	U_{eq}/U_{iso}
Li	4*d*	0.598(2)	0.109(1)	1/4							167(18)
Rh1	4*d*	0.09493(7)	0.19478(3)	1/4	67(2)	57(1)	54(1)	0	0	2(1)	59(1)
Rh2	8*e*	0.64646(5)	0.94766(2)	0.57811(2)	84(1)	71(1)	67(1)	1(1)	$-8(1)$	9(1)	74(1)
Sn1	4*d*	0.15705(6)	0.92428(3)	1/4	90(1)	60(1)	79(1)	0	0	$-14(1)$	76(1)
Sn2	8*e*	0.13329(4)	0.87304(2)	0.56292(2)	72(1)	85(1)	80(1)	$-2(1)$	8(1)	$-5(1)$	79(1)
Sn3	8*e*	0.62596(4)	0.67381(2)	0.88736(2)	97(1)	66(1)	75(1)	8(1)	9(1)	$-13(1)$	79(1)

Table 3. Interatomic distances (pm) of $LiRh_3Sn_5$ (standard deviations in parentheses), calculated with the powder lattice parameters. All distances of the first coordination sphere are listed.

Li:	2	Rh2	262.1(6)	Sn2:	1	Rh2	273.0(1)
	2	Sn2	280.1(6)		1	Rh1	277.0(1)
	1	Rh1	280.6(11)		1	Rh2	278.0(1)
	1	Rh1	284.0(11)		1	Li	280.1(6)
	1	Sn1	298.3(11)		1	Rh2	286.7(1)
	2	Sn3	300.9(9)		1	Sn2	289.2(1)
	2	Sn3	327.4(9)		1	Sn3	327.3(1)
	1	Sn1	335.2(11)		1	Sn2	328.7(1)
	1	Sn1	350.9(11)		1	Sn3	335.3(1)
Rh1:	1	Sn1	262.1(1)		1	Sn3	341.5(1)
	2	Sn3	264.5(1)		1	Sn1	347.7(1)
	1	Sn1	266.3(1)		1	Sn3	350.7(1)
	2	Sn2	277.0(1)		1	Sn3	356.7(1)
	1	Li	280.6(11)		1	Sn1	376.4(1)
	1	Li	284.0(11)	Sn3:	1	Rh1	264.5(1)
	2	Rh2	295.1(1)		1	Rh2	268.9(1)
Rh2:	1	Li	262.1(6)		1	Rh2	271.3(1)
	1	Sn3	268.8(1)		1	Rh2	271.4(1)
	1	Sn3	271.3(1)		1	Li	300.9(9)
	1	Sn3	271.4(1)		1	Sn1	322.3(1)
	1	Sn2	273.0(1)		1	Sn3	324.2(1)
	1	Sn1	274.1(1)		1	Sn2	327.3(1)
	1	Rh2	274.3(1)		1	Li	327.4(9)
	1	Sn2	278.0(1)		1	Sn2	335.3(1)
	1	Sn2	286.7(1)		1	Sn2	341.5(1)
	1	Rh1	295.1(1)		1	Sn1	349.2(1)
Sn1:	1	Rh1	262.1(1)		1	Sn2	350.7(1)
	1	Rh1	266.3(1)		1	Sn3	351.2(1)
	2	Rh2	274.1(1)		1	Sn2	356.7(1)
	1	Li	298.3(11)				
	2	Sn3	322.3(1)				
	1	Li	335.2(11)				
	2	Sn2	347.7(1)				
	2	Sn3	349.2(1)				
	1	Li	350.9(11)				
	2	Sn2	376.4(1)				

be obtained from Fachinformationszentrum Karlsruhe, D-76344 Eggenstein-Leopoldshafen (Germany), by quoting the Registry No. CSD-415529.

EDX analysis

The bulk sample and the single crystal measured on the diffractometer have been analyzed by EDX using a LEICA 420 I scanning electron microscope with elemental rhodium and tin as standards. The single crystal mounted on the quartz fibre was coated with a thin carbon film. Pieces of the bulk sample were polished with different silica and diamond pastes and left unetched for the analyses in the scanning electron microscope in backscattering mode. Neither metallic impurities nor tantalum contaminations from the crucible were detected *via* EDX. The analyses, 37 ± 2 at.-% Rh : 63 ± 2 at.-% Sn on average, were within the experimental uncertainties close to the ideal Rh : Sn ratio of 37.5 : 62.5 derived from the structure refinement.

Electronic structure calculations

Self-consistent DFT band structure calculations were performed using the LMTO-method in its scalar-relativistic version (program TB-LMTO-ASA) [31]. Detailed descriptions are given elsewhere [32, 33]. Reciprocal space integrations were performed with the tetrahedron method [34] using 45 *k*-points (grid of $8 \times 4 \times 4$) within the irreducible wedge of the Brillouin zone. The basis sets consisted of Li-$2s/\{2p/3d\}$ Rh-$5s/5p/4d/\{4f\}$ and Sn-$5s/5p/\{5d/4f\}$. Orbitals given in parentheses were downfolded [35]. In order to achieve space filling within the atomic sphere approximation, interstitial spheres were introduced to avoid too large overlap of the atom-centred spheres. The empty spheres positions and radii were calculated automatically. We did not allow overlaps of more than 15% for any two atom-centred spheres. The COHP method was used for the bond analysis [36]. COHP gives the energy contributions of all electronic states for a selected bond. The values are negative for bonding and pos-

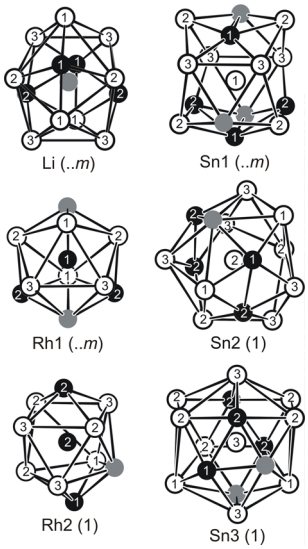

Fig. 1. Coordination polyhedra in the structure of $LiRh_3Sn_5$. All neighbors listed in Table 3 are drawn. The lithium, rhodium, and tin atoms are drawn as medium grey, black filled, and open circles, respectively. The site symmetries are indicated.

itive for antibonding interactions. With respect to the COOP diagrams, we plot –COHP(E) to get positive values for bonding states.

Results and Discussion

$LiRh_3Sn_5$ crystallizes with a new structure type with one lithium, two rhodium, and three crystallographically independent tin sites. The coordination polyhedra of all sites are presented in Fig. 1. The lithium atoms occupy relatively large cavities of coordination number (CN) 13 with four rhodium and nine tin neighbours. Due to the low lithium content, there are no Li–Li contacts in $LiRh_3Sn_5$ (the shortest Li–Li distance is 500 pm).

The shortest interatomic distance in the $LiRh_3Sn_5$ structure is the Li–Rh2 distance at 262 pm, similar to the Li–Rh distances (260 and 261 pm) in binary $LiRh_3$ [37]. However, these Li–Rh distances are longer than the sum of the covalent radii of 248 pm [38]. An even longer Li–Rh distance of 284 pm is observed in $LiRhSn_4$ [17]. The lithium atoms have the relatively high coordination number 13. The CN of lithium in intermetallics seems to be higher than in ionic compounds. Similar high coordination numbers have been observed in the stannides $LiTSn_4$ (T = Ru, Rh, Ir) [17] (LiT_2Sn_8, CN 10, in the form of a bi-capped square prism), $LiAg_8$ cubes (CN 8) in $LiAg_2Sn$ [23], CN 12 in Li_2AuSn_2 [21] (2 Li + 3 Au + 7 Sn), and a hexagonal prismatic lithium coordination in LiAuSn [23].

The 13 nearest neighbours of the lithium atoms in $LiRh_3Sn_5$ cover the relatively broad range of distances from 262 to 351 pm. Nevertheless, the lithium atoms are more or less centred within this coordination polyhedron. The CN 13 polyhedra are condensed *via* common Sn_3 triangles in the *b* direction, forming one-dimensional strands (Fig. 2) which are further condensed *via* Rh–Sn and Sn–Sn contacts.

Both rhodium sites have coordination number 10 (2 Li + 2 Rh + 6 Sn for Rh1 and 1 Li + 2 Rh + 7 Sn for Rh2). The Rh–Sn distances range from 262 to 287 pm, close to the sum of the covalent radii (265 pm) [38]. Similar Rh–Sn distances occur in the networks of $LiRhSn_4$ (280 pm) [17], GdRhSn (274 – 283 pm) [39], or $CeRhSn_2$ (262 – 277 pm) [40]. We can thus assume a considerable degree of Rh–Sn bonding in $LiRh_3Sn_5$. Each rhodium atom has two rhodium neighbours at Rh1–Rh2 of 295 and Rh2–Rh2 of 274 pm, leading to zig-zag chains that extend in the *c* direction (shown in Fig. 2). Both Rh–Rh distances are only slightly longer than in *fcc* rhodium (269 pm) [41].

Finally we need to discuss the tin coordination spheres. Due to their size, the tin atoms have the

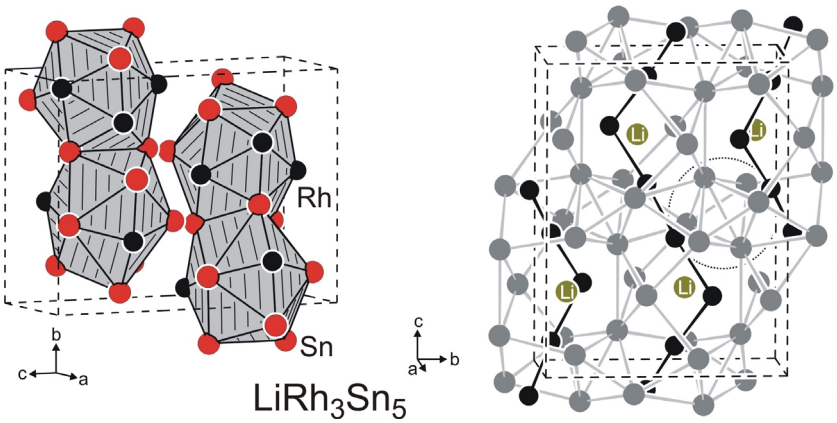

Fig. 2. Condensation of the CN 13 polyhedra around the lithium atoms (left hand part) and cutout of the tin substructure (right-hand part) in $LiRh_3Sn_5$. The rhodium and tin atoms are drawn as dark grey and black circles, respectively. One column of trans-edge sharing Sn_4 tetrahedra is encircled in the right-hand drawing.

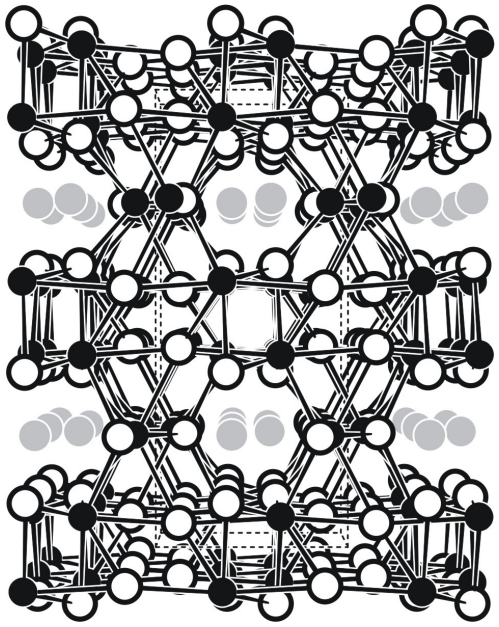

Fig. 3. View of the $LiRh_3Sn_5$ structure along the *b* axis (*c* up). The lithium, rhodium and tin atoms are drawn as medium grey, black, and open circles, respectively. The complex three-dimensional $[Rh_3Sn_5]$ network is emphasized.

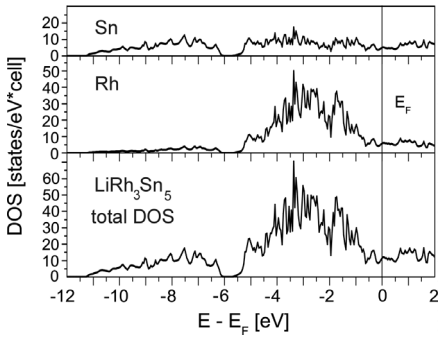

Fig. 4. Total and partial density-of-states for $LiRh_3Sn_5$. The energy zero is taken at the Fermi level.

highest coordination numbers (15, 14, and 15 for Sn1, Sn2, and Sn3, respectively). Each tin atom has between eight and nine tin neighbors at Sn–Sn distances covering the large range of distances from 289 to 376 pm. The shorter Sn–Sn distances compare well with the Sn–Sn distances in α- (281 pm) and β-Sn (4×302 and 2×318 pm) [41]. A cutout of the tin substructure is shown at the right-hand part of Fig. 2. As emphasized in that Figure, most tin atoms build up chains of trans-edge sharing tetrahedra along the *a* axis. Such tetrahedra also occur in the stannides $LiTSn_4$ (*T* = Ru, Rh, Ir) [17].

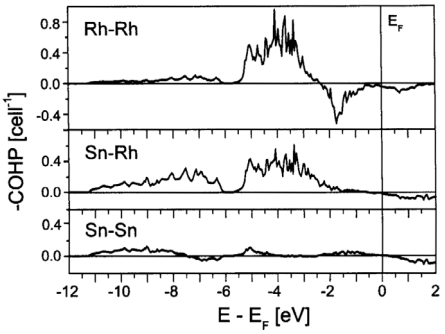

Fig. 5. Crystal Orbital Hamilton Populations (COHP) of selected bonds in $LiRh_3Sn_5$. Each curve applies to one average bond.

Together, the rhodium and tin atoms build up a rigid three-dimensional $[Rh_3Sn_5]$ network, in which the lithium atoms fill channels in the *b* direction (Fig. 3). The lithium atoms are connected to this network *via* the relatively short Li–Rh2 contacts (262 pm). Considering the electronegativities on the Pauling scale (Li: 0.98; Rh: 2.28; Sn: 1.96) [38], the lithium atoms as the most electropositive components must have largely lost their valence electrons, enabling covalent bonding within the $[Rh_3Sn_5]$ network. From this point of view it is reasonable to describe $LiRh_3Sn_5$ with a covalent $[Rh_3Sn_5]^{\delta-}$ polyanionic network, separated and charge balancing positively polarized lithium atoms, $Li^{\delta+}$.

We have investigated the electronic structure and chemical bonding in $LiRh_3Rn_5$ by density-of-states (DOS) and crystal orbital Hamilton populations (COHP), obtained from self consistent DFT band structure calculations. The total DOS and also the rhodium and tin partial DOS are shown in Fig. 4. No gap is discernible at the Fermi level in agreement with the metallic properties of $LiRh_3Sn_5$. The calculated DOS at E_F is 11 states/eV and roughly composed by 5% lithium, 52% rhodium and 45% tin orbitals. The DOS between -12 and -6 eV is dominated by the Sn-5*s* levels, which are considerably broadened and have therefore no lone pair character. Also the Rh-4*d* orbitals show strong energy broadening from -6 to -0.5 eV, which indicates that both the tin 5*s*, 5*p* as well as the rhodium 4*d* orbitals are strongly mixed and involved in chemical bonding. The integration of the DOS reveals about nine electrons in the ASA sphere of rhodium, 3.5 in the tin and 1.5 in the Li sphere. From this we infer that the electronic charge distribution in $LiRh_3Sn_5$ is relatively homoge-

neous and that polar contributions are small. However, it is not possible to determine reliable atomic charges from DOS integrations, because the integrated amount of charge depends on the ASA radii of concern. In the present case, we find 1.5 electrons inside the sphere around lithium, but this is not to equate with $Li^{0.5-}$, because the automatically generated ASA radius for Li in $LiRh_3Sn_5$ is rather large (2.97 au) due to the high coordination number. We think that the lithium atoms are not completely ionized to Li^+, but positively polarized due to their low electronegativity. The formulation $Li^{\delta+}[Rh_3Sn_5]^{\delta-}$ seems a good description. On the other side, the effect of no electron or at the most one electron transferred to the covalently bonded $[Rh_3Sn_5]$ network is surely very small.

Fig. 5 shows the COHP diagrams of the Rh−Rh, Rh−Sn and Sn−Sn bonds. For better comparison, each graph displays the averaged COHP of the bonds which form the coordination polyhedra. The completely filled Rh−Sn bonding states produce the by far strongest bonds in $LiRh_3Sn_5$. Their integration gives the ICOHP bonding energy of 1.7 eV/bond$_{Rh-Sn}$, similar to what we found in $LiRhSn_4$ [18]. But also the Rh−Rh bonding plays a significant role in $LiRh_3Sn_5$. Even though a part of Rh−Rh antibonding levels is already occupied, the ICOHP is $\sim$ 1 eV/bond$_{Rh-Rh}$, that is, almost 60% of a Rh−Sn bond. In contrast to this, the Sn−Sn interactions are rather weak and the COHP values small (Fig. 5). The mean ICOHP is only 0.32 eV/bond$_{Sn-Sn}$, but one must keep in mind that there are many more Sn−Sn than Rh−Rh contacts in the structure, so that the bonds between the tin atoms also contribute significantly to the stability of $LiRh_3Sn_5$.

Acknowledgements

We thank H.-J. Göcke for the work at the scanning electron microscope and Dipl.-Ing. U. Ch. Rodewald for the intensity data collection. This work was supported by the Deutsche Forschungsgemeinschaft through SFB 458 "Ionenbewegung in Materialien mit ungeordneten Strukturen". P. S. is indebted to the NRW Graduate School of Chemistry for a PhD stipend.

[1] R. A. Huggins, in J. O. Besenhard (ed.): Handbook of Battery Materials, Wiley-VCH, Weinheim (1999).
[2] R. A. Dunlap, D. A. Small, D. D. MacNeil, M. N. Obrovac, J. R. Dahn, J. Alloys Compd. **289**, 135 (1999).
[3] O. Genser, J. Hafner, Phys. Rev. B **63**, 144204 (2001).
[4] G. R. Goward, N. J. Taylor, D. C. S. Souza, L. F. Nazar, J. Alloys Compd. **329**, 82 (2001).
[5] C. Lupu, J.-G. Mao, J. W. Rabalais, A. M. Guloy, J. W. Richardson (Jr.), Inorg. Chem. **42**, 3765 (2003).
[6] F. Yin, X. Su, Zh. Li, J. Wang, J. Alloys Compd. **393**, 105 (2005).
[7] P. E. Lippens, J.-C. Jumas, J. Olivier-Fourcade, Hyp. Int. **156/157**, 327 (2004).
[8] H.-U. Schuster, Naturwissenschaften **53**, 360 (1966).
[9] H. Pauly, A. Weiss, H. Witte, Z. Metallkd. **59**, 47 (1968).
[10] H.-U. Schuster, D. Thiedemann, H. Schönemann, Z. Anorg. Allg. Chem. **370**, 160 (1969).
[11] C.-J. Kistrup, H.-U. Schuster, Z. Naturforsch. **27b**, 324 (1972).
[12] C.-J. Kistrup, H.-U. Schuster, Z. Anorg. Allg. Chem. **410**, 113 (1974).
[13] W. Pobitschka, H.-U. Schuster, Z. Naturforsch. **33b**, 115 (1978).
[14] U. Eberz, W. Seelentag, H.-U. Schuster, Z. Naturforsch. **35b**, 1341 (1980).
[15] J. Drews, U. Eberz, H.-U. Schuster, J. Less-Common Met. **116**, 271 (1986).
[16] C. Lupu, C. Downie, A. M. Guloy, Th. A. Albright, J.-G. Mao, J. Am. Chem. Soc. **126**, 4386 (2004).
[17] Zh. Wu, R.-D. Hoffmann, R. Pöttgen, Z. Anorg. Allg. Chem. **628**, 1484 (2002).
[18] Zh. Wu, H. Eckert, J. Senker, D. Johrendt, G. Kotzyba, B. D. Mosel, H. Trill, R.-D. Hoffmann, R. Pöttgen, J. Phys. Chem. B **107**, 1943 (2003).
[19] P. Sreeraj, H.-D. Wiemhöfer, R.-D. Hoffmann, R. Skowronek, A. Kirfel, R. Pöttgen, J. Mater. Chem., submitted.
[20] Zh. Wu, R.-D. Hoffmann, D. Johrendt, B. D. Mosel, H. Eckert, R. Pöttgen, J. Mater. Chem. **13**, 2561 (2003).
[21] Zh. Wu, B. D. Mosel, H. Eckert, R.-D. Hoffmann, R. Pöttgen, Chem. Eur. J. **10**, 1558 (2004).
[22] Zh. Wu, H. Eckert, B. D. Mosel, R. Pöttgen, Z. Naturforsch. **58b**, 501 (2003).
[23] R.-D. Hoffmann, D. Johrendt, Zh. Wu, R. Pöttgen, J. Mater. Chem. **12**, 676 (2002).
[24] P. Sreeraj, R.-D. Hoffmann, Zh. Wu, R. Pöttgen, U. Häussermann, Chem. Mater. **17**, 911 (2005).
[25] R. Pöttgen, Zh. Wu, R.-D. Hoffmann, G. Kotzyba, H. Trill, J. Senker, D. Johrendt, B. D. Mosel, H. Eckert, Heteroatom Chem. **13**, 506 (2002).
[26] R.-D. Hoffmann, Zh. Wu, R. Pöttgen, Eur. J. Inorg. Chem. 3425 (2003).
[27] R. Pöttgen, Th. Gulden, A. Simon, GIT Labor Fachzeitschrift **43**, 133 (1999).
[28] K. Yvon, W. Jeitschko, E. Parthè, J. Appl. Crystallogr. **10**, 73 (1977).

[29] G. M. Sheldrick, SHELXS-97, Program for the Determination of Crystal Structures, University of Göttingen, Germany (1997).
[30] G. M. Sheldrick, SHELXL-97, Program for Crystal Structure Refinement, University of Göttingen, Germany (1997).
[31] O. K. Andersen, O. Jepsen, Tight-Binding LMTO Vers. 4.7, Max-Planck-Institut für Festkörperforschung, Stuttgart (1994).
[32] O. Jepsen, M. Snob, O. K. Andersen, Linearized Band Structure Methods and its Applications, Springer Lecture Notes, Springer-Verlag, Berlin (1987).
[33] H. L. Skriver, The LMTO Method, Springer-Verlag, Berlin (1984).
[34] O. K. Andersen, O. Jepsen, Solid State Commun. **9**, 1763 (1971).
[35] W. R. L. Lambrecht, O. K. Andersen, Phys. Rev. B **34**, 2439 (1986).
[36] R. Dronskowski, P. Blöchl, J. Phys. Chem. **97**, 8617 (1993).
[37] H. C. Donkersloot, J. H. N. van Vucht, J. Less-Comon Met. **50**, 279 (1976).
[38] J. Emsley, The Elements, Oxford University Press, Oxford (1999).
[39] K. Łątka, R. Kmieć, R. Kruk, A. W. Pacyna, Th. Fickenscher, R.-D. Hoffmann, R. Pöttgen, J. Solid State Chem. **178**, 2077 (2005).
[40] D. Niepmann, R. Pöttgen, B. Künnen, G. Kotzyba, C. Rosenhahn, B. D. Mosel, Chem. Mater. **11**, 1597 (1999).
[41] J. Donohue, The Structures of the Elements, Wiley, New York (1974).